Editors' Suggestion

Ab initio prediction of nontrivial topological band and superconductivity in stable metallic Si allotropes at ambient pressure

Yoon-Gu Kang,[1] In-Ho Lee,[2,*] Myung Joon Han,[1] and Kee Joo Chang[1]
[1]*Department of Physics, Korea Advanced Institute of Science and Technology, Daejeon 34141, Korea*
[2]*Korea Research Institute of Standards and Science, Daejeon 34113, Korea*

(Received 22 July 2021; accepted 4 October 2021; published 13 October 2021)

Based on first-principles density functional calculations, we report the existence of both nontrivial band topology and superconductivity in three metallic Si allotropes, termed *Cmcm*-Si_4, *Cmmm*-Si_4, and *I*4/*mmm*-Si_4. *Cmcm*-Si_4 and *I*4/*mmm*-Si_4 are predicted in this study, whereas *Cmmm*-Si_4 was proposed in previous theoretical calculations. These metastable allotropes retain their crystalline structure at ambient pressure and exhibit superconductivity at the critical temperatures of 1.2–11.4 K. We investigate the topological characteristics of the electronic states and find the weak topological nature for all three allotropes. For *Cmcm*-Si_4, in particular, the formation of the surface Dirac point is clearly identified. Our result provides a promising platform for realizing a topological superconducting state in all-Si systems at ambient pressure.

DOI: 10.1103/PhysRevMaterials.5.104802

I. INTRODUCTION

Silicon (Si) is one of the most abundant elements in the Earth's crust and plays a key role in modern electronic devices. The cubic diamond (*cd*) phase of Si is semiconducting and thermodynamically most stable at ambient conditions. Si also exists in various metallic phases under compression, following the transition from *cd*-Si sequentially to β-Sn, *Imma*-Si, simple hexagonal (*sh*), *Cmca*-Si, hexagonal close-packed (*hcp*), and face-centered cubic (*fcc*) [1–5]. Upon pressure release from the high-pressure β-Sn phase, the other metastable phases such as rhombohedral R8, body-centered BC8 [6,7], and two unidentified Si-VIII and Si-IX [8] are obtained. Subsequent thermal annealing leads to a hexagonal diamond structure [6,7]. In addition, allotropes called BT8 and ST12 have been recently discovered using ultrafast laser-induced confined microexplosion [9]. All of these metastable phases are semiconducting and maintain their crystal structures at ambient conditions.

As an alternative, various metastable Si allotropes can be obtained from chemical precursors followed by physical and chemical manipulations. Theoretical and experimental studies have shown that chemical precursors can be produced at high pressure and/or high temperature for Li-Si, Na-Si, K-Si, Rb-Si, Ca-Si, and Ba-Si systems [10–16]. Particularly, for Na-Si systems, it is well known that type-I Si_{46} and type-II Si_{136} clathrates are synthesized by removing Na from the cages of Na_8Si_{46} and $Na_{24}Si_{136}$ precursors, respectively, while it is more difficult to completely remove Na from Na_8Si_{46} [17,18]. Recently, based on a fascinating high-pressure technique, an open-framework *Cmcm*-Si_6 allotrope was successfully synthesized by Na degassing from Na_4Si_{24} clathrate prepared at high temperature, and its crystal structure was maintained even after the pressure was released to ambient pressure [19]. In the type-I Si_{46}, type-II Si_{136}, and *Cmcm*-Si_6 clathrates, all Si atoms are fourfold coordinated, forming sp^3-like hybridization, and therefore these clathrates exhibit the semiconducting band structure.

Since the coordination number increases under compression, all high-pressure phases are metallic and some of them (β-Sn, *sh*, and *hcp*) have been shown to be superconducting under pressure [20–23]. However, the synthesis of stable metallic phases at ambient conditions has not been reported yet. Very recently, theoretical calculations predicted a new metallic allotrope, termed *P*6/*m*-Si_6, which is stable and superconducting at ambient pressure [24]. *P*6/*m*-Si_6 was suggested to be obtained by the pressure release and then the removal of Na from a *P*6/*m*-$NaSi_6$ clathrate which can be made at high pressure, similar to *Cmcm*-Si_6.

In all-Si systems, the topological characteristics of the electronic states have been demonstrated for only a few allotropes. A well-known two-dimensional allotrope is silicene, a graphene analog for silicon. Silicene is a Dirac semimetal in the absence of spin-orbit coupling (SOC), and it actually becomes a topological insulator with including SOC [25–28]. Self-encapsulated silicene, in which silicene is embedded between Si(110) layers in the cubic diamond lattice with sp^3 hybridization, also exhibits the band topology of Dirac semimetals [29]. Another single-layer Si allotrope in the *Cmma* structure is also a nodal loop semimetal without SOC [30]. Regarding three-dimensional structures, a number of low-density Si allotropes have been proposed based on advances in structure prediction [31–33]. Most of them have the semiconducting band structure, but two open-framework allotropes with a zeolite framework, termed AHT-Si_{24} and VFI-Si_{36}, have been recently proposed to be topological nodal line semimetals without SOC [33].

In this work, we report through first-principles theoretical calculations that three metallic Si allotropes, termed

*ihlee@kriss.re.kr

Cmcm-Si_4, *Cmmm*-Si_4, and *I*4/*mmm*-Si_4, exhibit a nontrivial band topology. The calculated $\mathbb{Z}_2$ topological invariants indicate a weak topological nature for these three allotropes. We suggest that the topological nature of their electronic states is more readily detectable in the surface band structure of *Cmcm*-Si_4 through angle-resolved photoemission experiments. We find that all three Si allotropes retain their crystal structure at ambient pressure and exhibit the superconducting behavior with the critical temperatures of 1.2–11.4 K.

II. METHODS

The structural and electronic properties of *Cmcm*-Si_4, *Cmmm*-Si_4, and *I*4/*mmm*-Si_4 were investigated using first-principles density functional calculations, in which the functional form of Perdew, Burke, and Ernzerhof (PBE) for the exchange-correlation potential [34] and the projector augmented wave potentials were employed [35], as implemented in the VASP code [36]. The wave functions were expanded in plane waves up to an energy cutoff of 500 eV. For Brillouin zone (BZ) integration, a set of **k** points was generated using a grid spacing of $2\pi \times 0.02$ Å^{-1}. The atomic coordinates and the lattice parameters were fully optimized until the residual forces and stress tensors were less than 0.01 eV/Å and a few kbar, respectively. It is noted that a high-energy cutoff is required for accurate stress tensor calculations.

To investigate the topological nature of the electronic states, we obtained maximally localized Wannier functions using the WANNIER90 code [37]. The topological surface states and Wannier charge center evolution ($\mathbb{Z}_2$ index) were calculated using the WANNIERTOOLS code [38]. For Si allotropes with inversion symmetry, the topological $\mathbb{Z}_2$ and $\mathbb{Z}_4$ indices were independently calculated using the QEIRREPS program [39], which employs the irreducible representation of Bloch wave functions. We calculated the full phonon spectrum and explored the superconductivity of *Cmcm*-Si_4, *Cmmm*-Si_4, and *I*4/*mmm*-Si_4 by calculating the electron-phonon coupling constant based on density functional perturbation theory, as implemented in the QUANTUM ESPRESSO package [40].

III. RESULTS AND DISCUSSION

A *Cmcm*-Si_4 allotrope (space group No. 63) was generated using a database-based structure search protocol [41]. Generative model machine learning techniques are used to find multiple crystal structures whose radial distribution functions are well compared with those of the known materials in the database. Namely, the radial distribution function was used to represent the general characteristics of the known Si crystal structures in the Materials Project database [42]. Then, the space of crystal structures was expanded using the variational autoencoder, which generates a set of representative crystal replicas, and the various random crystal structures were independently generated in terms of the crystal symmetry and atomic positions. Finally, to measure the degree of similarity between two crystal structures, we used the Pearson's distance between their radial distribution functions [41]. By choosing the criterion of 0.13 for the Pearson's distance, which ensures about 90% similarity, we were able to select various crystal structures by comparing their radial distribution functions with those of the known and replicated crystals. In particular, we found a crystal structure (space group No. 141) that has the Pearson's distance of 0.124 in comparison to the known structure of mp-1072544 in the Materials Project database. This structure, however, turns out to be the *Cmcm*-Si_4 allotrope after the atomic positions and cell shape are fully relaxed. On the other hand, for Li-Si systems, crystal structure search calculations showed that *Cmmm*-$LiSi_4$ is enthalpically stable under compression, and proposed that a *Cmmm*-Si_4 allotrope (space group No. 65) can be obtained by removing Li from the *Cmmm*-$LiSi_4$ precursor at ambient pressure [10,11].

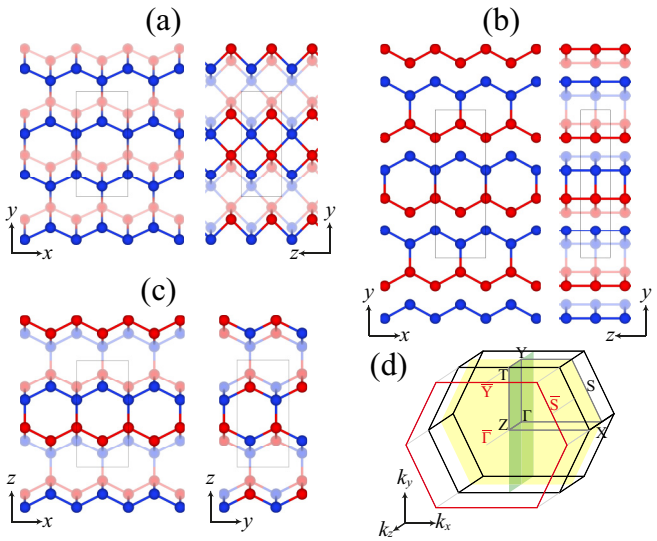

FIG. 1. Top and side views of the atomic structures of (a) *Cmcm*-Si_4, (b) *Cmmm*-Si_4, and (c) *I*4/*mmm*-Si_4. The *x*, *y*, and *z* axes follow the [100], [010], and [001] directions of the conventional cell, respectively, so the *y* and *z* axes are converted to each other in *I*4/*mmm*-Si_4. Dark and light circles in red and blue colors represent different planes made up of atoms. (d) The bulk BZ of the orthorhombic structure of *Cmcm*-Si_4 and *Cmmm*-Si_4 and the surface BZ projected onto the (001) plane drawn with high-symmetry points.

The atomic structures of *Cmcm*-Si_4, *Cmmm*-Si_4, and *I*4/*mmm*-Si_4 are shown in Fig. 1. The orthorhombic *Cmcm*-Si_4 structure consists of two interpenetrating honeycomblike sublattices. One sublattice is displaced by (0, 0.1873, 0.5) with respect to the other in the conventional orthorhombic cell with the lattice constants (*a*, *b*, *c*). The *Cmcm*-Si_4 is composed of fourfold and sixfold Si atoms and contains open channels along the crystallographic *c* axis, which are formed by six-membered Si rings. At ambient pressure, *Cmcm*-Si_4 has the equilibrium lattice constants $a = 4.428$, $b = 9.273$, and $c = 3.542$ Å, and two inequivalent Wyckoff positions, 4*cm*2*m* (0, 0.2137, 0.25) and 4*cm*2*m* (0, 0.5990, 0.25) (Table I). The *Cmmm*-Si_4 allotrope also forms an orthogonal structure containing hexagonal open channels along the *c* axis, similar to *Cmcm*-Si_4. It is interesting to note that *Cmmm*-Si_4 can be derived from *Cmcm*-Si_4 if one honeycomblike sublattice of *Cmcm*-Si_4 is displaced by $c/2$ along the *z* direction, followed by lattice relaxations such as stretching and compression in the *y* and *z* directions, respectively. The calculated equilibrium lattice constants of *Cmmm*-Si_4 are found to be $a = 4.383$, $b = 12.700$, and $c = 2.498$ Å, result-

TABLE I. Lattice parameters and Wyckoff positions for *Cmcm*-Si_4, *Cmmm*-Si_4, and *I*4/*mmm*-Si_4.

Allotrope	a (Å)	b (Å)	c (Å)	α (°)	β (°)	γ (°)	Wyckoff positions
Cmcm-Si_4	4.428	9.273	3.542	90.0	90.0	90.0	4 *c* *m*2*m* (0, 0.2137, 0.25) 4 *c* *m*2*m* (0, 0.5990, 0.25)
Cmmm-Si_4	4.383	12.700	2.498	90.0	90.0	90.0	4 *i* *m*2*m* (0, 0.8127, 0) 4 *i* *m*2*m* (0, 0.4033, 0)
*I*4/*mmm*-Si_4	4.361	4.361	9.103	90.0	90.0	90.0	4 *d* -4*m*2 (0, 0.5, 0.25) 4 *e* 4*mm* (0, 0.0, 0.372)

ing in a more compressed volume than *Cmcm*-Si_4. The crystal structure of *I*4/*mmm*-Si_4 (space group No. 139) is tetragonal with the equilibrium lattice constants $a = b = 4.361$ and $c = 9.103$ Å. We also note that *I*4/*mmm*-Si_4 can be derived from *Cmcm*-Si_4 if double zigzag chains toward the a axis of *Cmcm*-Si_4 are alternately displaced by $c/2$ in the z direction. The crystal volume of *I*4/*mmm*-Si_4 is significantly enhanced due to lattice elongation along one direction, leading to a low-density phase (Fig. 1 and Table I).

The total energies of *Cmcm*-Si_4, *Cmmm*-Si_4, and *I*4/*mmm*-Si_4 are plotted as a function of volume and compared with other Si allotropes in Fig. 2. We find that *Cmcm*-Si_4, *Cmmm*-Si_4, and *I*4/*mmm*-Si_4 are less stable than *cd*-Si, by having higher energies of 0.392, 0.368, and 0.363 eV/atom, respectively. High-density metallic phases are usually formed under pressure, but the β-Sn and *sh* phases do not hold when pressure is released. On the other hand, the metallic *P*6/*m*-Si_6 allotrope has a lower density and maintains its crystal structure at ambient pressure [24]. The *Cmcm*-Si_4, *Cmmm*-Si_4, and *I*4/*mmm*-Si_4 allotropes are also

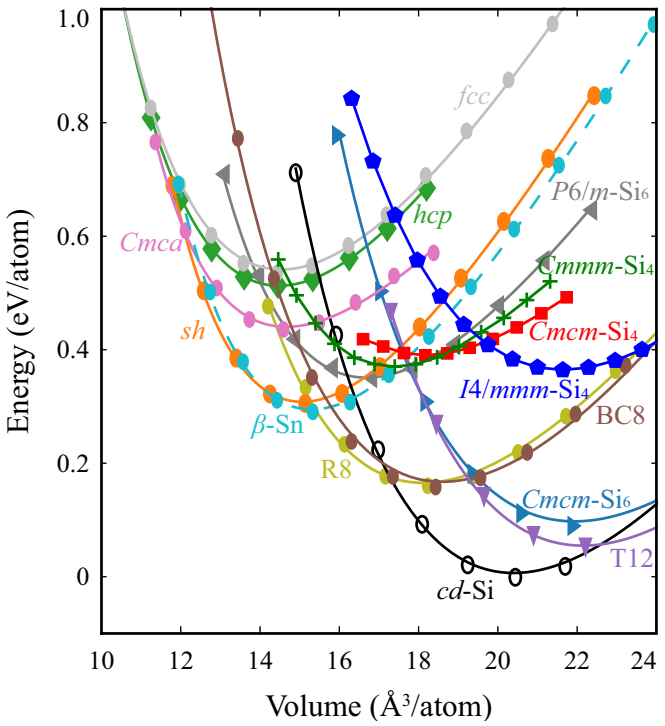

FIG. 2. Total energies of various Si allotropes including *Cmcm*-Si_4, *Cmmm*-Si_4, and *I*4/*mmm*-Si_4 plotted as a function of volume.

metallic (which will be discussed shortly), but they are less stable than the β-Sn, *sh*, and *P*6/*m*-Si_6 phases because of their lower density. Our results indicate that the energies of low-density metallic phases tend to increase with increasing crystal volume. For example, the equilibrium volumes of *sh*-Si, *P*6/*m*-Si_6, and *Cmcm*-Si_4 are 15.092, 16.714, and 18.181 Å^3/atom, respectively, and the energy of *Cmcm*-Si_4 is higher by 42 and 83 meV/atom, respectively, compared to *P*6/*m*-Si_6 and *sh*-Si. Despite the low density and high energy, *Cmcm*-Si_4, *Cmmm*-Si_4, and *I*4/*mmm*-Si_4 maintain their crystal structure at ambient pressure. We confirmed that the elastic constants C_{ij} meet the criteria for mechanical stability in both orthorhombic and tetragonal structures [43–45] (Table II). Also, the calculated phonon spectra show no imaginary modes in the BZ, indicating that *Cmcm*-Si_4, *Cmmm*-Si_4, and *I*4/*mmm*-Si_4 are all dynamically stable (Fig. 3).

Among these three allotropes, *Cmcm*-Si_4 is least stable and its crystal structure is more sensitive to pressure and temperature. The *Cmcm*-Si_4 allotrope is maintained only in a small range of pressure and easily converted to the *sh* phase as pressure increases. Using a generalized solid-state nudged elastic band method [46,47], we examined the structural transition from *Cmcm*-Si_4 to *sh*-Si and estimated the enthalpy barrier to be about 28 meV/atom at zero pressure (Fig. 4). As pressure increases, the enthalpy barrier tends to decrease and eventually disappears at around 7 GPa or more (Fig. 4). On the other hand, *Cmmm*-Si_4 and *I*4/*mmm*-Si_4 maintain their crystal structures even if pressure increases to 20 and 35 GPa, respectively. The thermal stability of three allotropes was examined by performing first-principles canonical ensemble molecular dynamics (*NVT*-MD) simulations at ambient pressure. For supercells containing 120 Si atoms for *Cmmm*-Si_4 and 128 Si atoms for *Cmcm*-Si_4 and *I*4/*mmm*-Si_4, *Cmmm*-Si_4 and *I*4/*mmm*-Si_4 were found to be stable up to 100 ps at temperatures of 810 and 560 K, respectively. The stability of *Cmcm*-Si_4 was maintained for temperatures up to 180 K, and its crystal structure turns to be a disordered one like amorphous Si when heated above 180 K.

Figures 5(a), 5(b), and 6(a) show the calculated band structure of *Cmcm*-Si_4, *Cmmm*-Si_4, and *I*4/*mmm*-Si_4, respectively. Their metallic nature is clearly noticed. All bands in the BZ have Kramers degeneracy due to inversion (P) and time-reversal (Θ) symmetry. For *Cmcm*-Si_4, in particular, several Dirac points can be identified near the Fermi level along high-symmetry lines in the absence of SOC. By including SOC, these Dirac points split with the band gaps of 8–13 meV [Fig. 6(a)]. To maintain the fourfold degeneracy, additional nonsymmorphic symmetry is needed [48–51]. The *Cmcm* space group consists of eight symmetry operations, including

TABLE II. Calculated elastic constants C_{ij} (in GPa) of *Cmcm*-Si_4, *Cmmm*-Si_4, and *I*4/*mmm*-Si_4. The elastic constants satisfy the criteria for mechanical stability in orthorhombic and tetragonal structures: $C_{11} > 0, C_{11}C_{22} > C_{12}^2, C_{11}C_{22}C_{33} + 2C_{12}C_{13}C_{23} - C_{11}C_{23}^2 - C_{22}C_{13}^2 - C_{33}C_{12}^2 > 0$, $C_{44} > 0$, $C_{55} > 0$, and $C_{66} > 0$ in an orthorhombic structure, whereas $C_{11} - C_{12} > 0$, $2C_{13}^2 < C_{33}(C_{11} + C_{12})$, $C_{44} > 0$, $C_{66} > 0$, and $2C_{16}^2 < C_{66}(C_{11} + C_{12})$ in a tetragonal structure.

Allotrope	C_{11}	C_{22}	C_{33}	C_{44}	C_{55}	C_{66}	C_{12}	C_{13}	C_{23}
Cmcm-Si_4	147.10	119.16	109.73	33.59	8.02	33.58	60.97	63.10	8.92
Cmmm-Si_4	205.60	145.33	300.06	26.29	69.00	26.46	77.07	−3.59	25.81
*I*4/*mmm*-Si_4	108.73	108.73	140.78	36.93	36.93	36.23	68.13	40.17	40.17

identity, inversion, two mirror reflections (M_x and $\hat{M}_z = \{M_z \mid \frac{1}{2}\hat{z}\}$), glide reflection ($G_y = \{M_y \mid \frac{1}{2}\hat{z}\}$), two twofold rotations (C_{2x} and $\hat{C}_{2y} = \{C_{2y} \mid \frac{1}{2}\hat{z}\}$), and twofold screw rotation ($S_{2z} = \{C_{2z} \mid \frac{1}{2}\hat{z}\}$). Among them, the inversion and two reflections of M_x and $\hat{M}_z$ play the key role in determining the nontrivial topological band character. It is noteworthy that $\hat{M}_z$ and $\hat{C}_{2y}$ are off-centered nonsymmorphic symmetries [49,52]. In the *Cmcm* space group, all nonsymmorphic operators have a half-lattice translation along the z axis, so that $k_z = 0$ and π/c become two invariant planes. In the primitive cell used here, the anticommutation relation is satisfied only in the $k_z = \pi/c$ plane between the nonsymmorphic symmetries and the product of inversion and time-reversal symmetries ($P\Theta$). The symmetry lines that host Dirac points are not in the $k_z = \pi/c$ plane, implying that these Dirac points are not protected in the presence of SOC. Therefore, the splitting of the Dirac points likely indicates the nontrivial band topology of *Cmcm*-Si_4.

For *Cmcm*-Si_4 with inversion symmetry, we examined the topological index, based on the irreducible representation of Bloch wave functions [39]. The $\mathbb{Z}_4$ invariant was calculated to be 2, indicating that *Cmcm*-Si_4 has either higher-order or weak topological nature. To investigate

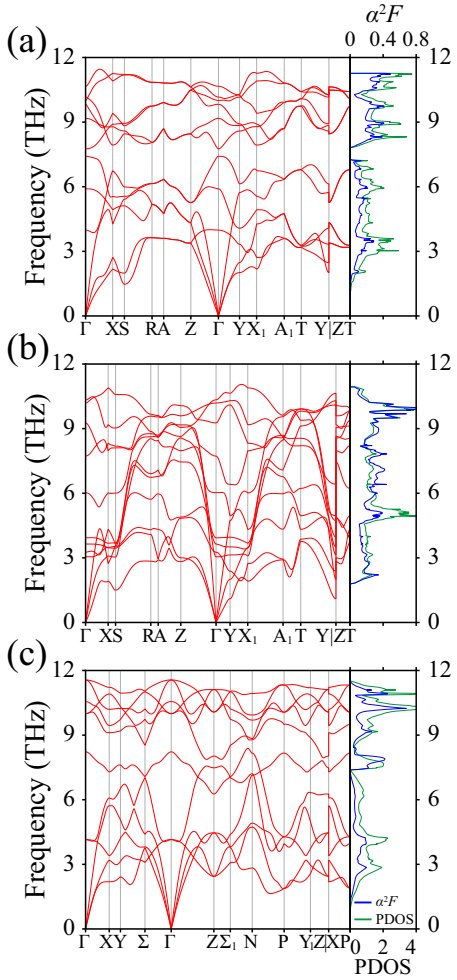

FIG. 3. Phonon spectra, phonon densities of states (PDOS in arbitrary units), and Eliashberg spectral functions $\alpha^2F(\omega)$ for (a) *Cmcm*-Si_4, (b) *Cmmm*-Si_4, and (c) *I*4/*mmm*-Si_4.

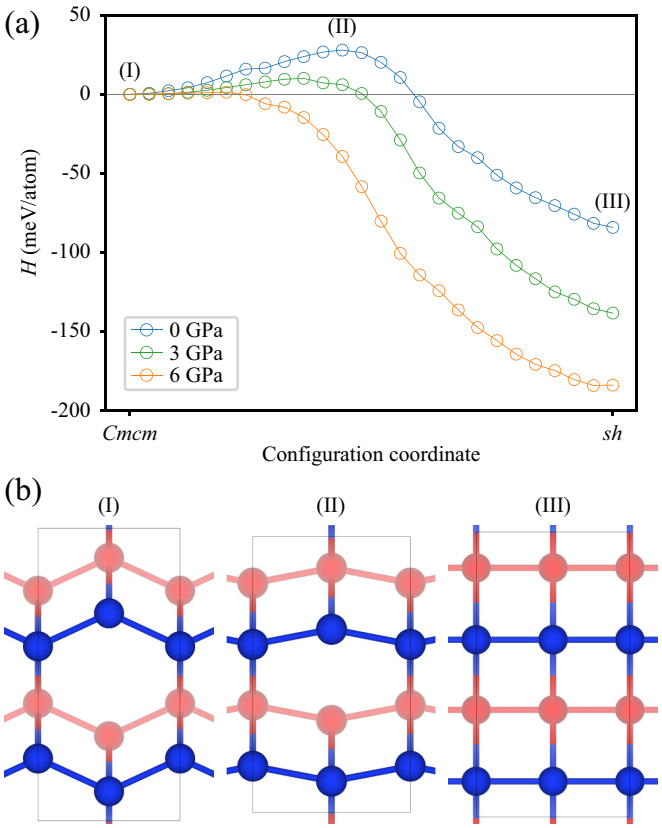

FIG. 4. (a) The variation of enthalpy during the structural transition from *Cmcm*-Si_4 to *sh*-Si is plotted as a function of configuration coordinate for different pressures using the generalized solid-state nudged elastic band method. The enthalpy barriers are calculated to be 28, 10, and 1 meV at 0, 3, and 6 GPa, respectively. (b) The atomic structures projected onto the (001) plane of *Cmcm*-Si_4 are shown for the initial, intermediate, and final configurations.

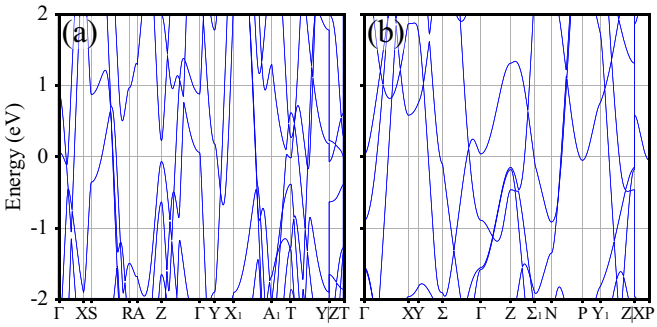

FIG. 5. Band structures without SOC of (a) *Cmmm*-Si_4 and (b) $I4/mmm$-Si_4 along the high-symmetry lines in the BZ of the primitive cell, with the Fermi level setting to zero.

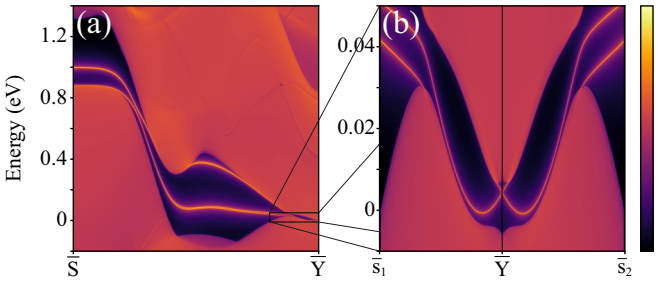

FIG. 7. (a) Surface electronic structure of *Cmcm*-Si_4 along the $\overline{S}$-$\overline{Y}$ line in the (001) surface BZ. The Kramers pairs switch partners between the $\overline{S}$ and $\overline{Y}$ points. In (b), the $\bar{s}_1$ and $\bar{s}_2$ points represent ± 0.2 $\overline{S}$ with respect to the $\overline{Y}$ point, respectively.

the $\mathbb{Z}_2$ topological invariant, we performed Wannier charge center calculations on time-reversal invariant momentum (TRIM) planes. From the flow of Wannier charge centers, four independent three-dimensional topological invariants are obtained, $(\nu_0;\nu_1\nu_2\nu_3) = (0;110)$, indicative of weak topological nature. Thus, the *Cmcm*-Si_4 crystal is characterized by a symmetry-based indicator $X_{BS} = (\nu_1, \nu_2, \nu_3, \mu_1) = (1, 1, 0, 2)$ that respects both inversion and time-reversal symmetries [53]. For *Cmmm*-Si_4 and $I4/mmm$-Si_4, the flow of Wannier charge centers yields the topological invariants of $(\nu_0;\nu_1\nu_2\nu_3) = (0;001)$ and $(0;111)$, respectively, indicating that these two phases are also weakly topological in nature. The $\mathbb{Z}_4$ invariants were calculated to be 0 and 2 for *Cmmm*-Si_4 and $I4/mmm$-Si_4, respectively, also supporting the weak topological characteristics.

To visualize the formation of topological surface states in *Cmcm*-Si_4, we calculated the surface band structure projected onto the (001) surface using the Green's function method, in which maximally localized Wannier functions are employed. Time-reversal symmetry requires the twofold degeneracy of surface states at TRIM points. The simulated energy distribution map of the surface states is plotted along the high-symmetry line in the (001) surface BZ, where the surface states are clearly seen in the gap region (Fig. 7). At the $\overline{S}$ point, two Kramers pairs appear at 0.9 and 1.0 eV above the Fermi level and split along the $\overline{S}$-$\overline{Y}$ line. One surface state of each Kramers pair is connected to either the bulk conduction or valence band. The other surface states of Kramers pairs change the partners between $\overline{S}$ and $\overline{Y}$, and form a Dirac cone at the $\overline{Y}$ point, as shown in Fig. 7(b). The presence of the surface Dirac point clearly shows the topological electronic states of *Cmcm*-Si_4. On the other hand, for *Cmmm*-Si_4 and $I4/mmm$-Si_4, the topological surface states were not clearly identified because they are buried in the bulk bands.

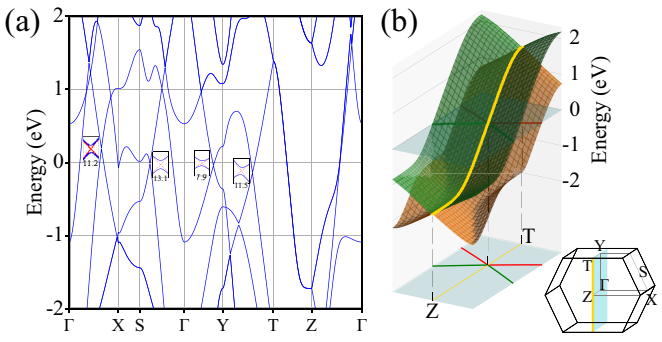

FIG. 6. (a) Band structure of *Cmcm*-Si_4 in the presence of SOC and (b) dispersive band on the Γ-*Z*-*T* plane, with the Fermi level setting to zero. In (a), insets show the enlarged view of the energy splitting at the Dirac points near the Fermi level. In (b), the Dirac nodal line along the *Z*-*T* symmetry line is highlighted in yellow.

In addition to the topological surface states, *Cmcm*-Si_4 exhibits a Dirac nodal line with the fourfold degeneracy along the *Z*-*T* line in the bulk BZ, as shown in Fig. 6(b). On the *Z*-*T* line invariant under two mirror reflections, M_x and $\hat{M}_z$, the Dirac nodal line is topologically protected by M_x and $\hat{M}_z$ in combination with inversion and time-reversal symmetry. When the primitive cell is chosen for *Cmcm*-Si_4, the Hamiltonian H satisfies three commutation relations with M_x, $\hat{M}_z$, and $P\Theta$ such that $[H, M_x] = 0$ for $k_x = 0$, $[H, \hat{M}_z] = 0$ for $k_z = 0$ and π/c, and $[H, P\Theta] = 0$ for all (k_x, k_y, k_z) vectors in the BZ. With SOC for a spin-1/2 system, $\hat{M}_z^2 = -1$. Thus, $\hat{M}_z$ has two eigenvalues $\pm i$ on the invariant planes, i.e., $\hat{M}_z|k_x, k_y, k_z\rangle_\pm = \pm i|k_x, k_y, k_z\rangle_\pm$ for $k_z = 0$ and π/c. It is important to note that the off-centered nonsymmorphic operator $\hat{M}_z$ anticommutes with $P\Theta$, $\{\hat{M}_z, P\Theta\} = 0$ for $k_z = \pi/c$, whereas the commutation relation is satisfied for $k_z = 0$. Due to the anticommutation relation between $\hat{M}_z$ and $P\Theta$ on the $k_z = \pi/c$ plane, $P\Theta|k_x, k_y, \pi/c\rangle_\pm$ has the same $\hat{M}_z$ eigenvalues $\pm i$ as $|k_x, k_y, \pi/c\rangle_\pm$, forming a Kramers pair that is orthogonal to each other.

To find other eigenstates of $\hat{M}_z$ on the $k_z = \pi/c$ plane, we consider the *Z*-*A* and *Z*-*T* symmetry lines which are specified by $(k_x, 0, \pi/c)$ and $(0, k_y, \pi/c)$, respectively. On the *Z*-*A* line invariant under $\hat{M}_z$ and G_y, the glide reflection G_y anticommutes with $P\Theta$, i.e., $\{G_y, P\Theta\} = 0$. Thus, $|k_x, 0, \pi/c\rangle_\pm$ and $P\Theta|k_x, 0, \pi/c\rangle_\pm$ have the same G_y eigenvalues $\pm i$. However, because G_y commutes with $\hat{M}_z$, i.e., $[G_y, \hat{M}_z] = 0$ on the $k_z = \pi/c$ plane, $G_y|k_x, 0, \pi/c\rangle_\pm$ and $P\Theta G_y|k_x, 0, \pi/c\rangle_\pm$ have the same $\hat{M}_z$ eigenvalues $\pm i$ as $|k_x, 0, \pi/c\rangle_\pm$ and $P\Theta|k_x, 0, \pi/c\rangle_\pm$. Since these four states do not satisfy the orthogonality, the fourfold degeneracy is not preserved along the *Z*-*A* line. On the other hand, $\hat{M}_z$ anticommutes with M_x, i.e., $\{\hat{M}_z, M_x\} = 0$, on the *Z*-*T* line which is invariant under $\hat{M}_z$ and M_x. In fact, the anticommutation relation between $\hat{M}_z$ and M_x is satis-

TABLE III. Crystal volumes (V), densities of states at the Fermi level [$N(0)$], electron-phonon coupling constants (λ), logarithmic average of phonon frequencies ($\omega_{\log}$), and superconducting critical temperatures (T_c) for $Cmcm$-Si_4, $Cmmm$-Si_4, and $I4/mmm$-Si_4, in comparison with sh-Si and $P6/m$-Si_6 [24].

Allotrope	Pressure (GPa)	V (Å^3/atom)	$N(0)$ (states/Ry/atom/spin)	λ	$\omega_{\log}$ (K)	T_c (K)
sh-Si	15	13.50	2.44	0.660	250	7.9
$P6/m$-Si_6	0	16.80	2.40	0.799	263	12.2
$Cmcm$-Si_4	0	18.18	1.87	0.462	253	2.2
$Cmmm$-Si_4	0	17.38	2.52	0.808	238	11.4
$I4/mmm$-Si_4	0	21.64	1.87	0.417	234	1.2

fied regardless of k vectors. For $M_x|0, k_y, \pi/c\rangle_\pm$ and $P\Theta M_x|0, k_y, \pi/c\rangle_\pm$, we find the opposite $\hat{M}_z$ eigenvalues $\mp i$ due to the anticommutation relation of $\{\hat{M}_z, M_x\} = 0$. The four orthogonal eigenstates of $\hat{M}_z$ are $|0, k_y, \pi/c\rangle_\pm$, $P\Theta|0, k_y, \pi/c\rangle_\pm$, $M_x|0, k_y, \pi/c\rangle_\pm$, and $P\Theta M_x|0, k_y, \pi/c\rangle_\pm$, all of which share the same eigenvalue of the Hamiltonian. Thus, with the inversion and time-reversal symmetries, the fourfold degeneracy along the Z-T line is topologically protected by $\hat{M}_z$ and M_x in the $Cmcm$-Si_4 allotrope.

The superconductivity of Si was observed in the metallic β-Sn, sh, and hcp phases under pressure, with the critical temperatures of 4–8 K [20–23]. Type-I clathrates of $(Na,Ba)_xSi_{46}$ and Ba_8Si_{46} exhibit superconductivity under ambient conditions [54–56], while the Si_{46} clathrate with metal ions removed from the cages is a semiconductor [32]. The metallic $P6/m$-Si_6 allotrope was theoretically proposed to be superconducting with the critical temperature of about 12 K at zero pressure [24]. We explored the superconductivity of $Cmcm$-Si_4 by calculating the electron-phonon coupling constant λ from a density-functional perturbation theory, as implemented in the QUANTUM ESPRESSO code [40]. The electron-phonon interaction matrix was calculated using the $4 \times 4 \times 4$ phonon-momentum grids, and a denser $16 \times 16 \times 16$ grid was used to perform the BZ integration. The electron-phonon coupling $\lambda_{\boldsymbol{q}\nu}$ at a phonon wave vector $\boldsymbol{q}$ for a phonon mode ν is related to the phonon linewidth $\gamma_{\boldsymbol{q}\nu}$, $\lambda_{\boldsymbol{q}\nu} = \gamma_{\boldsymbol{q}\nu}/[2\pi\omega^2_{\boldsymbol{q}\nu}N(0)]$, where $N(0)$ is the density of states at the Fermi level and $\omega_{\boldsymbol{q}\nu}$ is the phonon frequency. The logarithmic average of phonon frequencies, $\omega_{\log}$, and the frequency-dependent electron-phonon coupling $\lambda(\omega)$ were calculated from the Eliashberg spectral function $\alpha^2F(\omega)$, $\lambda(\omega) = 2\int_0^\omega[\alpha^2F(\omega')/\omega']d\omega'$ (Fig. 3). For $Cmcm$-Si_4, we obtain the electron-phonon coupling constant of $\lambda = 0.462$, which is given by $\lambda = \lambda(\infty)$. By choosing the Coulomb pseudopotential of $\mu^* = 0.1$ in the Allen-Dynes modified McMillan equation [57], we estimate the superconducting critical temperature T_c to be about 2.2 K at zero pressure. The critical temperature of $Cmcm$-Si_4 is lower than that of β-Sn and sh phases, as well as the $P6/m$-Si_6 allotrope, mainly due to the smaller $N(0)$ (Table III). For $Cmmm$-Si_4, due to the larger $N(0)$, the higher critical temperature of 11.4 K is obtained at zero pressure, which is similar to $P6/m$-Si_6. For $I4/mmm$-Si_4, the small $\omega_{\log}$ and $N(0)$ lead to the lower T_c of 1.2 K.

Finally, we discuss a possible route for the synthesis of $Cmcm$-Si_4, $Cmmm$-Si_4, and $I4/mmm$-Si_4. It is known that various metastable Si allotropes can be obtained using a two-step high-pressure precursor method, in which a precursor filled with alkali or alkaline earth metals in the Si host structure is first synthesized at high pressure and then metal ions are removed from cages or open channels by thermal degassing. For example, in Na-Si systems, the semiconducting $Cmcm$-Si_6 clathrate has been successfully synthesized from the Na_4Si_{24} precursor made at high pressure [19]. In recent theoretical calculations for $NaSi_4$, two enthalpically stable phases were suggested to form under compression: $P\bar{1}$-$NaSi_4$ above 2 GPa and $P2/m$-$NaSi_4$ at about 12 GPa [12]. These two allotropes contain open channels, but their crystal structures are distinct from $Cmcm$-Si_4 and $Cmmm$-Si_4. In Li-Si systems, the $Cmmm$-$LiSi_4$ allotrope was predicted to be enthalpically stable under compression [10,11]. The $Cmmm$-$LiSi_4$ structure consists of hexagonal open channels, along which the Li atoms sandwiched between the Si layers are intercalated with 12-fold coordination. A stable $Cmmm$-Si_4 allotrope can be obtained by removing Li from $Cmmm$-$LiSi_4$ at ambient pressure [10,11].

If alkali metals (A = Li, Na, K, Rb, Cs) are inserted into the open channels of $Cmcm$-Si_4, ASi_4 compounds with a stoichiometry of 1:4 do not maintain the $Cmcm$ symmetry and form in a new orthorhombic structure of $Amm2$-ASi_4 (space group No. 38), where metal ions are intercalated between double zigzag Si chains, as shown in Fig. 8. For alkali metal-Si systems ASi_4, we calculated the enthalpies of $Amm2$-ASi_4, $Cmmm$-ASi_4, and $I4/mmm$-ASi_4 under pressure (Fig. 8). Then, we examined the energetics of these allotropes by comparing their enthalpies with those for other previously proposed allotropes, such as $I4/m$-$LiSi_4$ [10], $P\bar{1}$- and $P2/m$-$NaSi_4$ [12], and $C2/m$-$RbSi_4$ [14]. The $P\bar{1}$-ASi_4 phase is enthalpically favorable for all alkali metals in the low-pressure region. As pressure increases, the stable phase for A = Li changes to $Cmmm$-$LiSi_4$ and $I4/m$-$LiSi_4$ at 5 and 40 GPa, respectively, and $P2/m$-$NaSi_4$ is the most stable phase for A = Na above 20 GPa, in good agreement with the previous calculations [11,12]. For A = K, we find two stable phases under compression, $C2/m$-KSi_4 and $Cmmm$-KSi_4 at 30 GPa and 50 GPa, respectively. In a recent study of $RbSi_4$, three allotropes were theoretically predicted to form under compression, $Cmcm$-$RbSi_4$, $I4/mcm$-$RbSi_4$, and $C2/m$-$RbSi_4$ at 3.3, 11.4, and 26.2 GPa, respectively [14]. Similarly, we also find $C2/m$-$RbSi_4$ and $C2/m$-$CsSi_4$ allotropes at 30 GPa. We note that $Cmcm$-$RbSi_4$ has the same crystal symmetry as $Cmcm$-Si_4, but consists of a different arrangement of Si atoms. According to our calculations, $Cmmm$-Si_4 can be obtained when metal ions are removed from $Cmmm$-$LiSi_4$ or $Cmmm$-KSi_4; however, the synthesis of $Cmcm$-Si_4 and $I4/mmm$-Si_4 may require other appropriate experimental conditions.

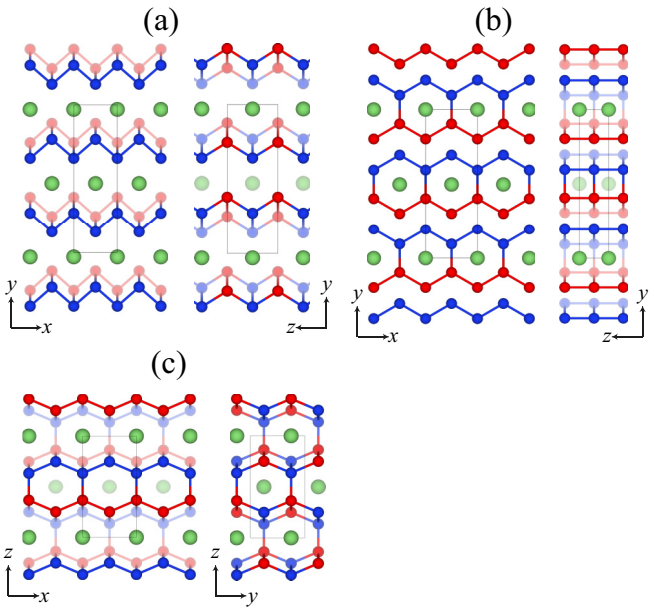

FIG. 8. Top and side views of the atomic structures of (a) *Amm*2-ASi_4, (b) *Cmmm*-ASi_4, and (c) $I4/mmm$-ASi_4 with A = Li, Na, K, Rb, and Cs. Dark and light circles in red and blue colors represent different planes made up of atoms.

IV. CONCLUSIONS

In conclusion, we have investigated the band topology and superconductivity of three metallic Si allotropes, called *Cmcm*-Si_4, *Cmmm*-Si_4, and $I4/mmm$-Si_4, through first-principles calculations. Among these metallic phases, the *Cmcm*-Si_4 and $I4/mmm$-Si_4 allotropes are predicted here, whereas *Cmmm*-Si_4 was proposed in the previous theoretical calculations [10,11]. Although the *Cmcm*-Si_4, *Cmmm*-Si_4, and $I4/mmm$-Si_4 structures are metastable with respect to cubic diamond Si as well as other known high-pressure metallic phases, they maintain their crystal structure at ambient pressure. We have verified the stability of *Cmcm*-Si_4, *Cmmm*-Si_4, and $I4/mmm$-Si_4 through molecular dynamics simulations, elastic constants, and phonon spectra calculations. By computing topological invariants, we found that all the metallic allotropes exhibit the weak topological nature in their electronic band structures. For *Cmcm*-Si_4, we have identified the formation of nontrivial surface states protected by time-reversal symmetry which can be observed in angle-resolved photoemission experiments. In addition, *Cmcm*-Si_4, *Cmmm*-Si_4, and $I4/mmm$-Si_4 are predicted to be superconducting with the critical temperatures of 1.2–11.4 K. Thus, the quantum phase transition from a nontrivial semimetal to a topological superconducting state is expected below 11.4 K. Our findings open a path to manipulate Si-based topological superconducting properties, hopefully helping to fabricate high-speed spintronic devices.

ACKNOWLEDGMENTS

Y.G.K., M.J.H., and K.J.C. were supported by Creative Materials Discovery Program through the NRF funded by the Ministry of Science and ICT (Grant No. 2018M3D1A1058754). I.H.L was supported by the National Center for Materials Research Data (NCMRD) through the National Research Foundation of Korea (NRF) funded by the Ministry of Science and ICT (NRF-2021M3A7C2089748). Y.G.K. and M.J.H. were supported by Basic Science Research Program through the NRF funded by the Ministry of Science and ICT (Grant No. 2021R1A2C1009303).

[1] J. Z. Hu and I. L. Spain, Solid State Commun. **51**, 263 (1984).
[2] S. J. Duclos, Y. K. Vohra, and A. L. Ruoff, Phys. Rev. B **41**, 12021 (1990).
[3] M. I. McMahon, R. J. Nelmes, N. G. Wright, and D. R. Allan, Phys. Rev. B **50**, 739 (1994).
[4] M. Hanfland, U. Schwarz, K. Syassen, and K. Takemura, Phys. Rev. Lett. **82**, 1197 (1999).
[5] S. Wippermann, Y. He, M. Vörös, and G. Galli, Appl. Phys. Rev. **3**, 040807 (2016).
[6] R. H. Wentorf, Jr. and J. S. Kasper, Science **139**, 338 (1963).
[7] J. Crain, G. J. Ackland, J. R. Maclean, R. O. Piltz, P. D. Hatton, and G. S. Pawley, Phys. Rev. B **50**, 13043(R) (1994).
[8] Y.-X. Zhao, F. Buehler, J. R. Sites, and I. L. Spain, Solid State Commun. **59**, 679 (1986).
[9] L. Rapp, B. Haberl, C. J. Pickard, J. E. Bradby, E. G. Gamaly, J. S. Williams, and A. V. Rode, Nat. Commun. **6**, 7555 (2015).
[10] S. Zhang, Y. Wang, G. Yang, and Y. Ma, ACS Appl. Mater. Interfaces **8**, 16761 (2016).
[11] W. Li, M. Lu, E. Zurek, X. Xu, L. Chen, M. Zhang, L. Gao, X. Zhong, J. Li, X. Zhou, and W. Liu, Phys. Lett. A **383**, 1047 (2019).
[12] S. Zhang, L. Chen, M. Zhang, L. Gao, X. Cui, D. Zhang, W. Li, Y. Tian, Y. Du, and J. Li, Phys. Lett. A **392**, 127146 (2021).
[13] C.-M. Hao, Y. Li, H.-M. Huang, and Y.-L. Li, J. Chem. Phys. **148**, 204706 (2018).
[14] X. Cui, X. Zhang, Y. Liu, Y. Xi, Y. Du, D. Zhang, and X. Wang, Comput. Mater. Sci. **198**, 110704 (2021).
[15] G. Gao, N. W. Ashcroft, M. Miao, and R. Hoffmann, J. Phys. Chem. C **118**, 25167 (2014).
[16] J. Shi, W. Cui, J. A. Flores-Livas, A. San-Miguel, S. Botti, and M. A. L. Marques, Phys. Chem. Chem. Phys. **18**, 8108(R) (2016).
[17] J. Gryko, P. F. McMillan, R. F. Marzke, G. K. Ramachandran, D. Patton, S. K. Deb, and O. F. Sankey, Phys. Rev. B **62**, R7707(R) (2000).
[18] S. Stefanoski, C. D. Malliakas, M. G. Kanatzidis, and G. S. Nolas, Inorg. Chem. **51**, 8686 (2012).
[19] D. Y. Kim, S. Stefanoski, O. O. Kurakevych, and T. A. Strobel, Nat. Mater. **14**, 169 (2015).
[20] W. Buckel and J. Wittig, Phys. Lett. **17**, 187 (1965).
[21] K. J. Chang, M. M. Dacorogna, M. L. Cohen, J. M. Mignot, G. Chouteau, and G. Martinez, Phys. Rev. Lett. **54**, 2375 (1985).

[22] G. Martinez, J. M. Mignot, G. Chouteau, K. J. Chang, M. M. Dacorogna, and M. L. Cohen, Phys. Scr. **T13**, 226 (1986).
[23] D. Erskine, P. Y. Yu, K. J. Chang, and M. L. Cohen, Phys. Rev. Lett. **57**, 2741 (1986).
[24] H.-J. Sung, W. H. Han, I.-H. Lee, and K. J. Chang, Phys. Rev. Lett. **120**, 157001 (2018).
[25] S. Cahangirov, M. Topsakal, E. Aktürk, H. Şahin, and S. Ciraci, Phys. Rev. Lett. **102**, 236804 (2009).
[26] C.-C. Liu, H. Jiang, and Y. Yao, Phys. Rev. B **84**, 195430 (2011).
[27] P. Miró, M. Audiffred, and T. Heine, Chem. Soc. Rev. **43**, 6537 (2014).
[28] M. Ezawa, J. Phys. Soc. Jpn. **84**, 121003 (2015).
[29] G.-M. Kim, H.-J. Sung, W. H. Han, I.-H. Lee, and K. J. Chang, J. Phys. Chem. C **123**, 1839 (2019).
[30] N. Zhou, P. Zhou, J. Li, C. He, and J. Zhong, Phys. Rev. B **100**, 115425 (2019).
[31] M. Amsler, S. Botti, M. A. L. Marques, T. J. Lenosky, and S. Goedecker, Phys. Rev. B **92**, 014101 (2015).
[32] M. Beekman, K. Wei, and G. S. Nolas, Appl. Phys. Rev. **3**, 040804 (2016).
[33] Z. Liu, H. Xin, L. Fu, Y. Liu, T. Song, X. Cui, G. Zhao, and J. Zhao, J. Phys. Chem. Lett. **10**, 244 (2019).
[34] J. P. Perdew, K. Burke, and M. Ernzerhof, Phys. Rev. Lett. **77**, 3865 (1996).
[35] G. Kresse and D. Joubert, Phys. Rev. B **59**, 1758 (1999).
[36] G. Kresse and J. Furthmüller, Comput. Mater. Sci. **6**, 15 (1996).
[37] G. Pizzi, V. Vitale, R. Arita, S. Blügel, F. Freimuth, G. Géranton, M. Gibertini, D. Gresch, C. Johnson, T. Koretsune, J. Ibañez-Azpiroz, H. Lee, J.-M. Lihm, D. Marchand, A. Marrazzo, Y. Mokrousov, J. I. Mustafa, Y. Nohara, Y. Nomura, L. Paulatto, S. Poncé, T. Ponweiser, J. Qiao *et al.* J. Phys.: Condens. Matter **32**, 165902 (2020).
[38] Q. S. Wu, S. N. Zhang, H.-F. Song, M. Troyer, and A. A. Soluyanov, Comput. Phys. Commun. **224**, 405 (2018).
[39] A. Matsugatani, S. Ono, Y. Nomura, and H. Watanabe, Comput. Phys. Commun. **264**, 107948 (2021).
[40] P. Giannozzi, O. Andreussi, T. Brumme, O. Bunau, M. B. Nardelli, M. Calandra, R. Car, C. Cavazzoni, D. Ceresoli, M. Cococcioni, N. Colonna, I. Carnimeo, A. Dal Corso, S. de Gironcoli, P. Delugas, R. A. DiStasio Jr, A. Ferretti, A. Floris, G. Fratesi, G. Fugallo, R. Gebauer, U. Gerstmann *et al.*, J. Phys.: Condens. Matter **29**, 465901 (2017).
[41] I.-H. Lee and K. J. Chang, Comput. Mater. Sci. **194**, 110436 (2021).
[42] A. Jain, S. P. Ong, G. Hautier, W. Chen, W. D. Richards, S. Dacek, S. Cholia, D. Gunter, D. Skinner, G. Ceder, and K. A. Persson, APL Mater. **1**, 011002 (2013).
[43] Z.-j. Wu, E.-j. Zhao, H.-p. Xiang, X.-f. Hao, X.-j. Liu, and J. Meng, Phys. Rev. B **76**, 054115 (2007).
[44] F. Mouhat and F.-X. Coudert, Phys. Rev. B **90**, 224104 (2014).
[45] S. Singh, I. Valencia-Jaime, O. Pavlic, and A. H. Romero, Phys. Rev. B **97**, 054108 (2018).
[46] G. Henkelman, B. P. Uberuaga, and H. Jónsson, J. Chem. Phys. **113**, 9901 (2000).
[47] D. Sheppard, P. Xiao, W. Chemelewski, D. D. Johnson, and G. Henkelman, J. Chem. Phys. **136**, 074103 (2012).
[48] J. W. Han, S.-W. Kim, W. S. Kyung, C. Kim, G. Cao, X. Chen, S. D. Wilson, S. Cheon, and J. S. Lee, Phys. Rev. B **102**, 041108(R) (2020).
[49] B.-J. Yang, T. A. Bojesen, T. Morimoto, and A. Furusaki, Phys. Rev. B **95**, 075135 (2017).
[50] J.-H. Park, S. H. Lee, C. H. Kim, H. Jin, and B.-J. Yang, Phys. Rev. B **99**, 195107 (2019).
[51] C. Fang, Y. Chen, H.-Y. Kee, and L. Fu, Phys. Rev. B **92**, 081201(R) (2015).
[52] C. J. Bradley and A. P. Cracknell, *The Mathematical Theory of Symmetry in Solids* (Clarendon Press, Oxford, 1972).
[53] H. C. Po, A. Vishwanath, and H. Watanabe, Nat. Commun. **8**, 50 (2017).
[54] H. Kawaji, H. O. Horie, S. Yamanaka, and M. Ishikawa, Phys. Rev. Lett. **74**, 1427 (1995).
[55] S. Yamanaka, E. Enishi, H. Fukuoka, and M. Yasukawa, Inorg. Chem. **39**, 56 (2000).
[56] D. Connétable, V. Timoshevskii, B. Masenelli, J. Beille, J. Marcus, B. Barbara, A. M. Saitta, G.-M. Rignanese, P. Mélinon, S. Yamanaka, and X. Blase, Phys. Rev. Lett. **91**, 247001 (2003).
[57] P. B. Allen and R. C. Dynes, Phys. Rev. B **12**, 905 (1975).